Afropolitan Journals

ISSN: 2762-4585X www.afropolitanjournals.com

Structural and Optical Study of Lithium Doped Sulphur Supported Reduced Graphene Oxide (Li_X:S-rGO_{1-X}) (0.4≤X≤0.6) Composite Electrode for Optoelectronics Applications

M. Alpha[1], Idris M. Bako[1], A. Z. Ngari[1], T. O. Daniel[2], Umar M. Muhammad[1], Muhammad Jaafar[1] and Idris A. Sulaimon[1]

[1]Department of Physics, Nigerian Army University Biu, Borno, Nigeria. [2]Department of Physics, Alex Ekwueme-Federal University Ndufu-Alike, Ebonyi State.

Corresponding author: alpha.matthew@naub.edu.ng

Abstract

The goal of this study was to developed a conducting Lithium doped sulfur supported reduced graphene oxide composites using hydrothermal reduction technique approach that allows the presence of different weight concentration of Li ion in network of supported reduced graphene oxide for application as electrode material. Scanning electron microscopy, X-ray diffraction, and UV Spectrometry analysis were each used to evaluate the produced composites. From the findings, it was possible to predict that the presence of a nano-size additive Li in the network of the S-rGO composite significantly improve the charge transport and dielectric characteristics of the material at the percolation threshold. The optical energy band gaps for S-rGO, $Li_{0.4}$:S-r$GO_{0.6}$, and $Li_{0.6}$:S-r$GO_{0.4}$ are, respectively, 3.4 eV, 3.5 eV, and 3.6 eV. These values are optimal and favour achieving the threshold voltage for optoelectronic and energy storage application.

Keywords: Electrode, Optoelectronics, Reduced Graphene Oxide, Lithium, Doped Sulfur Composite.

Introduction

Due to the distinguishing characteristics, such as stabilisation, anti-corrosive characteristics, simple acid/base doping/de-doping, being light-weight, and being relatively inexpensive for composite preparation, reduced grapheme oxide (rGO) filled nano-composites have recently attained a distinct importance in both science and academia. Depending on the level of protonation and the synthesis process, they show substantial physical changes (Nakazawa, *et al*., 2014; Siamak, *et al*., 2015). Li has most frequently been used in different composites with carbonaceous materials in a variety of technological applications, including sensors, electrodes for supercapacitors and optoelectronics. One such substance that has drawn a lot of interest since its discovery is graphene, which has a wide range of uses and incredibly intriguing features. A really fantastic material, graphene has the potential to create breakthrough technology. Subsequently graphene was first discovered in 2004, it has since been claimed to have a wide range of amazing properties (Alpha *et al*., 2019; Raymundo-Pinero *et al*., 2004; Martinelli *et al*., 2009).

For energy storage in optoelectronics, selection of electrode material is of paramount importance because it determines the electrical properties.

However, the main challenges towards the development of cheap and high performance electrode composites for optoelectronics are;

1. Lower achievable electrode charge surface area
2. Less expectation for cost reduction problems.

These challenges limit the electrical performance of the electrode. So their popularity among manufacturers seem to have progressively decreased, also their wider usage is highly limited by their charge surface area. Hence the need for the development of cheap and high performance electrode composite material.

Li and S-rGO are combined in different doping concentration with the intention of strengthening conducting electrode materials as well as creating intriguing electronic properties by morphological alteration and electronic interaction between components. There are many ways to make rGO composites, however one common technique that is frequently utilized is hydrothermal reduction technique. The composites used in this research are produced using this technique.

The elemental composition of the composite, morphology of the composite, and optical parameters were determined using energy dispersive x-ray spectroscopy, scanning electron microscopy (SEM), X–ray diffraction, and a UV Spectrophotometer analysis. The average crystallite size (D) can be computed using

$$D = \frac{0.9\lambda}{\beta\cos\theta} \quad (1)$$

Where θ = diffraction angle, λ = wavelength of the X-rays (1.5406 ˚A) and β = full width at half maximum (FWHM). Dislocation density δ was calculated from (Ilican *et al.*, 2008; Largeot *et a*l., 2008).

$$\delta = \frac{1}{D^2} \quad (2)$$

The micro-strain ε can be evaluated from (Mukherjee and Mitra, 2015)

$$\varepsilon = \frac{\beta}{4\tan\theta} \quad (3)$$

Where D, β and θ retain their meanings as defined for Eq. (1). The absorption coefficient α (alpha) can be calculated from (Mukherjee and Mitra, 2015)

$$\alpha = 2.303\frac{A}{t} \quad (4)$$

Methodology

Synthesis of reduced graphene oxide (rGO)

5 g of graphite was measured and another 2.5 g of sodium nitrate were added together. 115 ml of concentrated sulfuric acid was added to the mixture and sonicated at 60 °C for thirty minutes. The mixture was then transferred into an ice bathe, then 15 g of potassium permanganate was added slowly into the mixture and the temperature was maintained at below 20 °C, after the potassium permanganate was added, the temperature was then raised to 35 °C by sonication process for 20 min. 100 ml of distilled water and 1 g of ascorbic acid was added to the mixture slowly to aid reduction and the temperature was raised to 95 °C, then it was stirred for another 15 min. At the end of the 15 min, 100 ml of distilled water

and 10 ml of hydrogen peroxide was added to the mixture to aid homogeneity. The solution was then filtered and then washed with 1 M of hydrochloric acid (8.3 ml of hydrochloric acid mixed with 100 ml of distilled water gives 1 M) and 100 ml of distilled water. The residue was then mixed with polyvinyl chloride and 4 drops of toluene were used to bind the residue, it was then placed on slides in an electric oven at 60 °C for 8 hrs to dry, and graphene oxide was obtained.

Synthesis of Sulphur Supported Reduced Graphene Oxide (S-RGO)

Reduced Graphene Oxide was synthesised from graphite powder by modified Hummer's method as described by [1]. The rGO was synthesized by hydrothermal method. The rGO was grounded into powdered form then 100 ml of distilled water and 2 g of Thiourea was added to the solution as source of Sulphur, the mixture was then sonicated for 30 min at 60 °C. The mixture was transferred into a stainless-steel autoclave for the hydrothermal reaction at 160 °C for 6 hrs. The product was then collected and washed with distilled water and it was filtered. Finally, the residue was mixed with polyvinyl chloride and 4 drops of toluene and it was placed on slides in an electric oven at 60 °C for 6 hrs to dry. After it dries Sulphur supported reduced Graphene Oxide was obtained.

Synthesis of Lithium Doped Sulphur Supported Reduced Graphene Oxide (Li_X:S-rGO_{1-x}) (0.4≤X≤0.6)

Li_2CO_3 serves as source of Li and S-rGO were added to 100 ml of distilled water for the synthesis of Li_x:S-rGO_{1-x} (0.4≤X≤0.6) in the following compositions: $Li_{0.4}$:S-$rGO_{0.6}$, $Li_{0.6}$:S-$rGO_{0.4}$. the S-rGO cake was thoroughly grounded using an agate mortar and pestle, the mixture for each composition was sonicated for 30 min at 60 °C, after which it was transferred into a stainless-steel autoclave for hydrothermal reaction at 160 °C for 6 hrs. The pH was adjusted to neutral value using 50 ml of 0.1 M potassium hydroxide (1.12 g of potassium hydroxide diluted with 200 ml distilled water). The final product was collected, filtered and washed with distilled water. The mixtures were then mixed with polyvinyl chloride and 4 drops of toluene and it was placed on slides and then dried in an electric oven at 60 °C for 2 hrs. After it was dried, a composite of Li_x:S-rGO_{1-x} (0.4≤X≤0.6) was obtained.

Results

The XRD Results

Figure 1 shows the XRD pattern for S-rGO, $Li_{0.4}$:S-$rGO_{0.6}$ and $Li_{0.6}$:S-$rGO_{0.4}$ composites scanned across a 2 theta angle of 20° to 80° range utilising a CuKá1 X - ray source with a wavelength of 1.5406Å using an XPERT-PRO diffractometer from Panalytical (Netherlands) that was powered at 35 kV, 50 mA, and a scan rate of 0.02° per step.

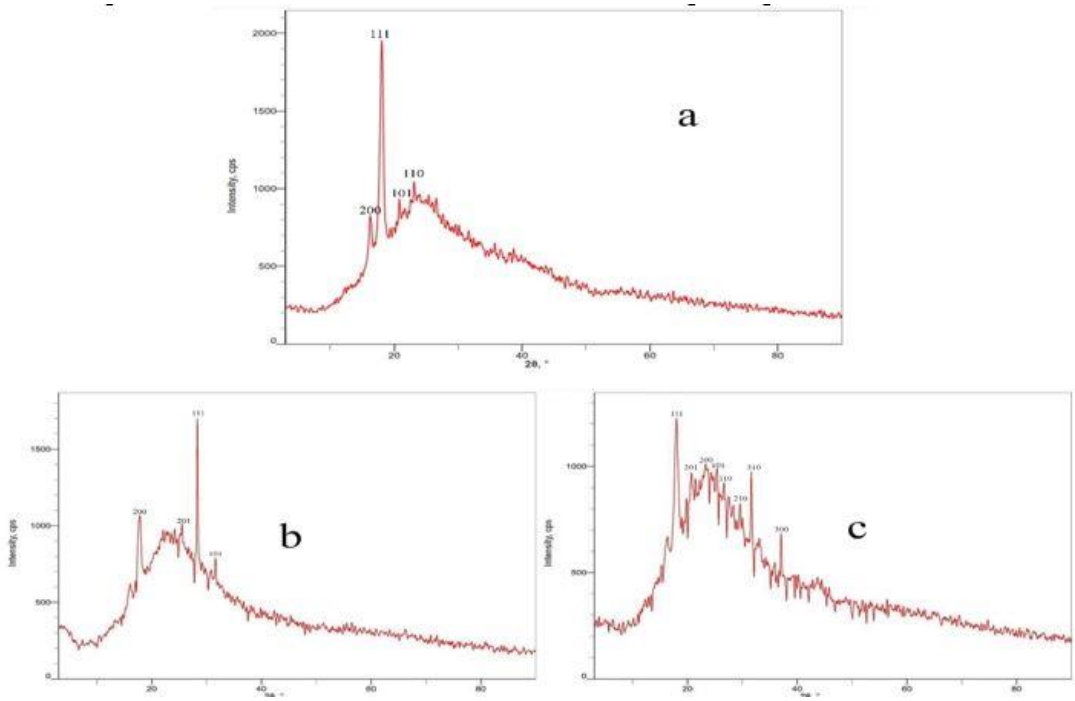

Figure 1: XRD Diffractogram for (a) S-rGO; (b) $Li_{0.4}$:S-rGO$o_{.6}$; (c) $Li_{0.6}$:S-r$GO_{0.4}$

Using the typical pattern for the mineral herzenbergite, the composites' peaks were analysed and indexed (JCPDS PDF card 39-0355). The XRD pattern reveals the formation of crystalline with few peaks. The peaks with the most preferred orientation diffracted along the reflection planes (111) for the corresponding composites S-rGO, $Li_{0.4}$:S-r$GO_{0.6}$ and $Li_{0.6}$:S-r$GO_{0.4}$, at 2 theta angles of 19.7°, 30.1°, and 30.9°, respectively and have a tetragonal rutile-type structure having intensity which is directly proportional to the number of diffracting particles (atoms) for the entire composite, regardless of the doping concentration. This suggests that the presence of the doped metal ion and the change in electron density in the conduction band, brought about by the addition of active cations (Li^+) into the network of S-rGO and have enhanced ordering of the material along the stacking direction. The smaller peaks point in the direction of stacking that is primarily composed of reduced graphene oxide this agrees with (Skoog *et al.*, 2016; Uwe and Neil, 2011). This is due to early crystallization. This favours the formation of atomic layers, increasing crystal size and reducing crystal defects in the network of the composite material.

The SEM Results

The SEM images and EDXs of S-rGO, $Li_{0.4}$:S-r$GO_{0.6}$ and $Li_{0.6}$:S-r$GO_{0.4}$ are shown in Figures 2, 3 and 4. All samples in this study had their surface morphology and microstructure examined using a Phenoworld Pro X Model scanning electron microscope (SEM) run in secondary electron detection mode at 2 kV. On the carbon double-sided tape that was fastened to an aluminium substrate holder, the samples were inserted.

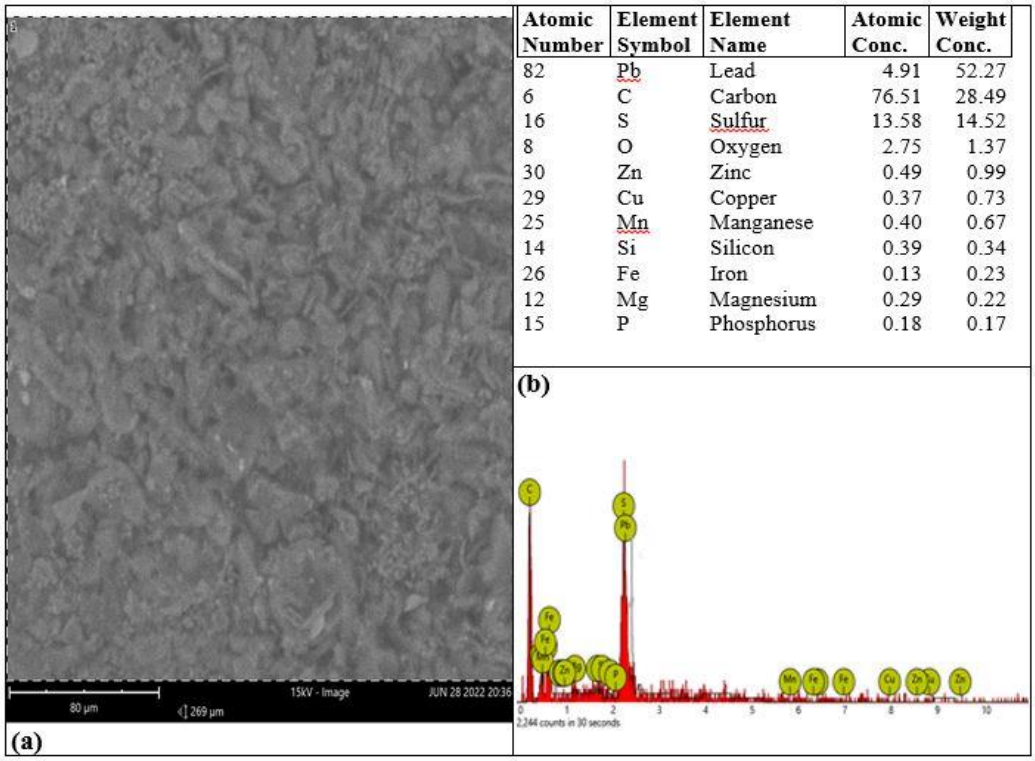

Atomic Number	Element Symbol	Element Name	Atomic Conc.	Weight Conc.
82	Pb	Lead	4.91	52.27
6	C	Carbon	76.51	28.49
16	S	Sulfur	13.58	14.52
8	O	Oxygen	2.75	1.37
30	Zn	Zinc	0.49	0.99
29	Cu	Copper	0.37	0.73
25	Mn	Manganese	0.40	0.67
14	Si	Silicon	0.39	0.34
26	Fe	Iron	0.13	0.23
12	Mg	Magnesium	0.29	0.22
15	P	Phosphorus	0.18	0.17

Figure 2: (a) SEM Image and (b) EDX for S-rGO

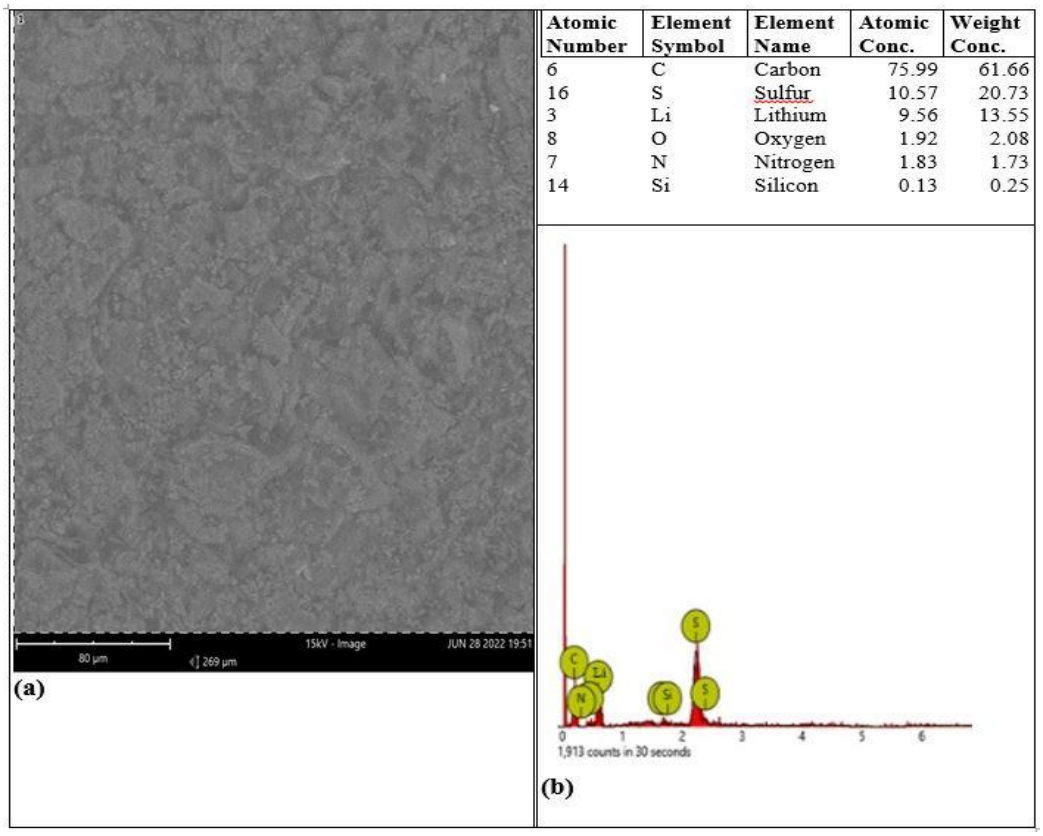

Atomic Number	Element Symbol	Element Name	Atomic Conc.	Weight Conc.
6	C	Carbon	75.99	61.66
16	S	Sulfur	10.57	20.73
3	Li	Lithium	9.56	13.55
8	O	Oxygen	1.92	2.08
7	N	Nitrogen	1.83	1.73
14	Si	Silicon	0.13	0.25

Figure 3: (a) SEM Image and (b) EDX for $Li_{0.4}$:S-r$GO_{0.6}$

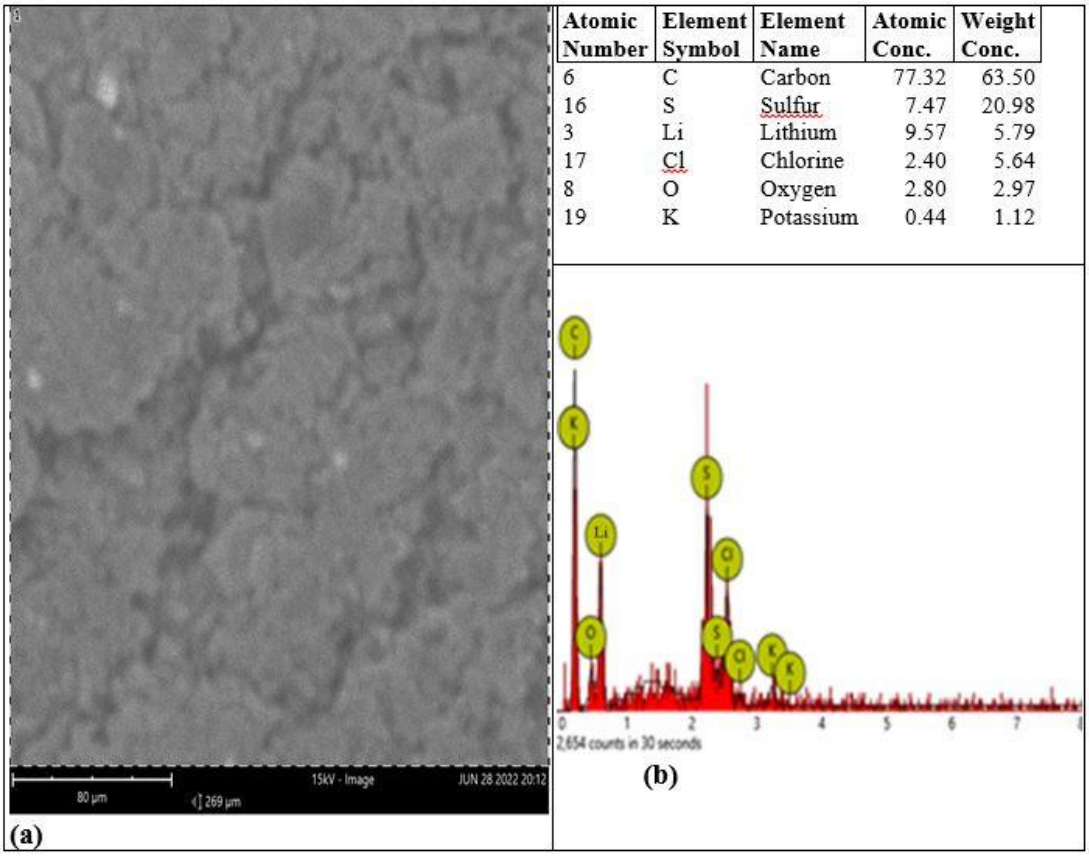

Atomic Number	Element Symbol	Element Name	Atomic Conc.	Weight Conc.
6	C	Carbon	77.32	63.50
16	S	Sulfur	7.47	20.98
3	Li	Lithium	9.57	5.79
17	Cl	Chlorine	2.40	5.64
8	O	Oxygen	2.80	2.97
19	K	Potassium	0.44	1.12

Figure 4: (a) SEM Image and (b) EDX for $Li_{0.6}$:S-r$GO_{0.4}$

As seen in the SEM image in figures 3 and 4, the doped metal oxide is chemically encapsulated between the layers of the sulfur supported reduced graphene oxide, generating a 3D architectural composite material with excellent distribution. For the doped composites, the SEM images revealed very uniform porous surface structures, which are seen to grow with an increase in the doping concentration.

With increasing dopant concentration, the surface coalescence breaks down, as shown in the SEM image by a modest increase in the number of grain boundaries. However, because all the samples were created under the same conditions, independent of the doping concentration, a nearly identical microstructure and surface morphology were observed in all the doped electrode composites. The enhanced electrochemical utilization of Li and S nanoparticles into the network of the composite electrode are made possible by the interaction of reduced graphene oxide layers via van der Waals forces (Uwe and Neil, 2011), which create an open pore system that allows electrolyte ions to readily access the surfaces of the composite.

Optical Characterisation

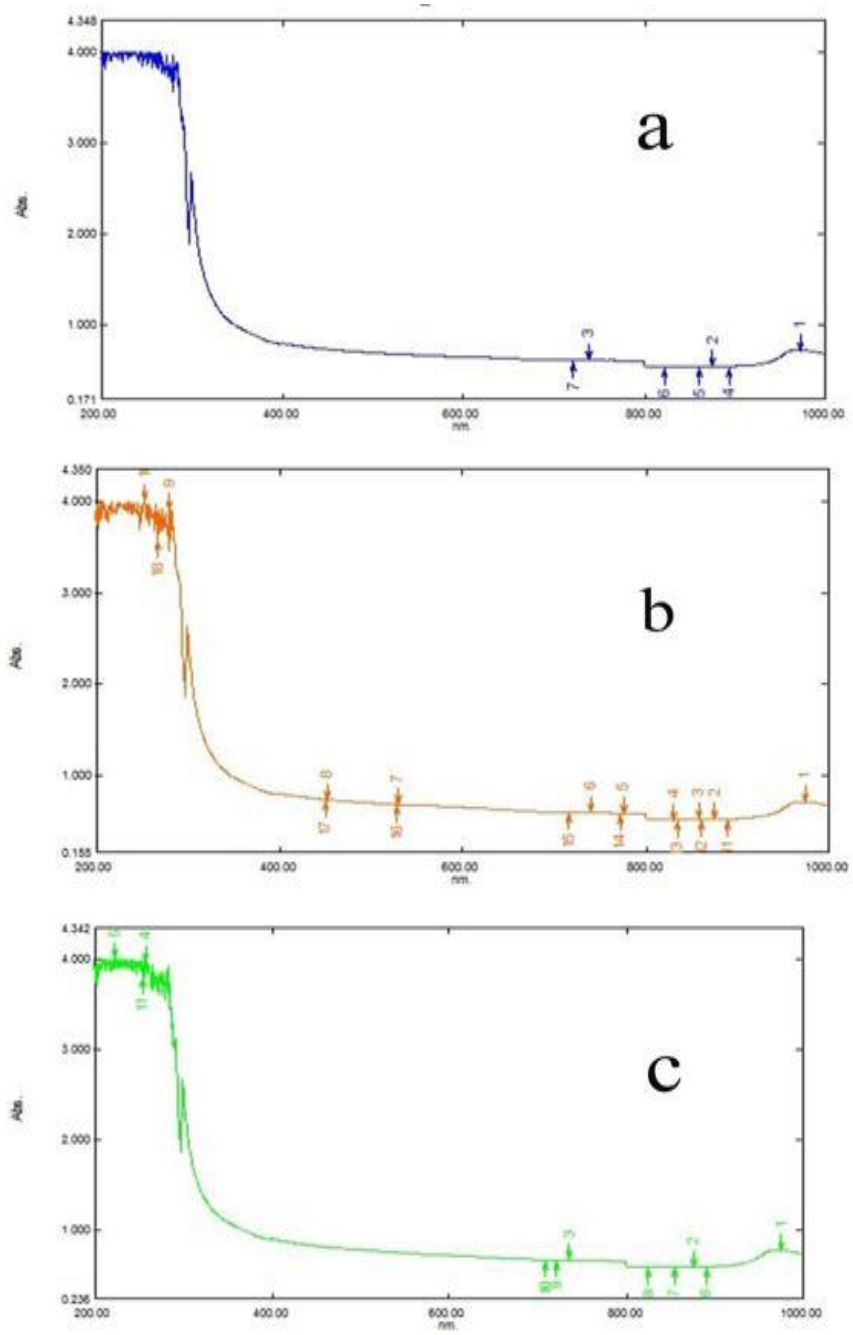

Figure 5: UV Spectra: (a) S-rGO; (b) $Li_{0.4}$:S-rGO$o_{.6}$; (c) $Li_{0.6}$:S-rGO$_{0.4}$

The normalising spectrum for the UV spectrum in figure 5 above allows us to more easily see shift in peaks in the location of wavelength. The spectra in figure 5 indicated that smaller particle sizes are closer to the shorter blue wavelength of light i.e blue-shifted and the larger particle sizes are closer to the longer wavelength of light i.e red-shifted.

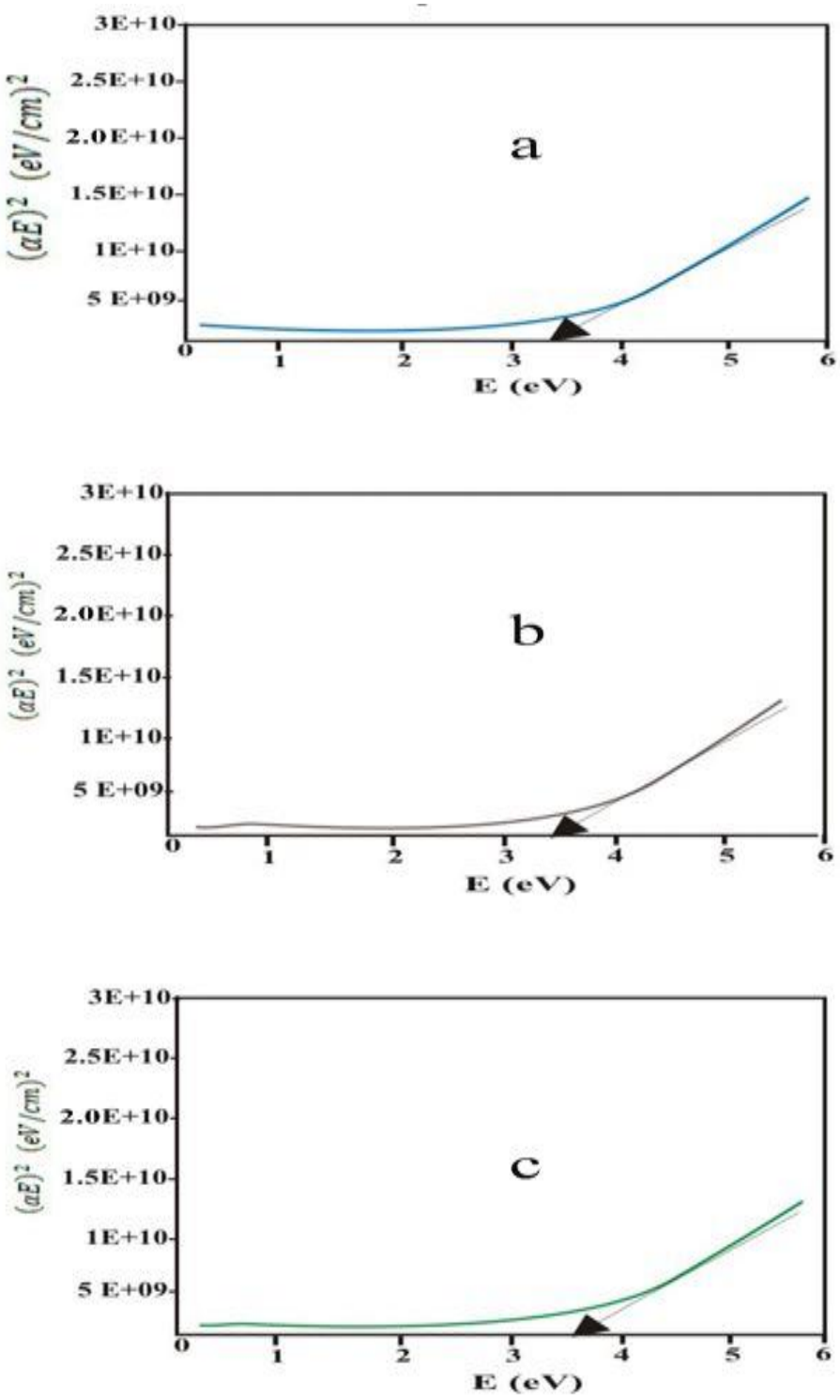

Figure 6: Tauc Plot: for (a) S-rGO; (b) $Li_{0.4}$:S-$rGO_{0.6}$; (c) $Li_{0.6}$:S-$rGO_{0.4}$

This red-shifted and blue-shifted is caused by absorption of radiation which causes the promotion of electrons from the ground state to the excited state in functional groups called chromophore. Electron excitation that occurs in UV-VIS spectrophotometry is

recorded in the form of a spectrum expressed as wavelength and absorbance, according to the type of electrons present in the composite material (Uwe and Neil, 2011; Daniel, *et al*., 2019). The easier the electrons to excite, the more electrons are excited and the higher the absorbance as seen in the figure 5. As the particle size get larger the optical density goes down, this is as a result of the increase in number of particles during the doping of Li. As the Li ion are released from the surface, the ionic Li is reduced and self-nucleated to form new particles. The optical band gap (E_g) and absorption coefficient are related by the Tauc plot as reported by (Uwe and Neil, 2011; Daniel, *et al*., 2019), where the symbols retain their usual meaning:

$$(\alpha h\nu)^{\frac{1}{p}} = A(h\nu - E_g) \quad (5)$$

The optical band gap (E_g) of S-rGO, $Li_{0.4}$:S-$rGO_{0.6}$ and $Li_{0.6}$:S-$rGO_{0.4}$ were obtained by extrapolating a straight line from the $(\alpha h\nu)^2$ vs E_g plots to the $(\alpha h\nu)^2 = 0$ axis, where the intersection point gives the optical band gap. Figure 6 gives the Tauc's plot from which the optical band gap (E_g) was estimated. The band gap for S-rGO, $Li_{0.4}$:S-$rGO_{0.6}$ and $Li_{0.6}$:S-$rGO_{0.4}$ are 3.4 eV, 3.5 eV and 3.6 eV respectively. The increase in the band gap was as a result of increase in the Li ion concentration in the network of the composite material, this agrees with (Deshmukh *et al*., 2015; Nakazawa, *et al*., 2014).

Conclusion

From the findings, it was possible to predict that the presence of a nano-size additive Li in the network of the S-rGO composite significantly improve the charge transport and dielectric characteristics of the material at the percolation threshold. The optical energy band gaps for S-rGO, $Li_{0.4}$:S-$rGO_{0.6}$, and $Li_{0.6}$:S-$rGO_{0.4}$ are, respectively, 3.4 eV, 3.5 eV, and 3.6 eV. These values are optimal and favour achieving the threshold voltage for optoelectronic and energy storage application.

Acknowledgments

The authors acknowledged the support Central Laboratory, Department of Chemistry, Nigerian Army University Biu.

Funding

This research did not receive any specific grant/funds from any funding agencies.

Conflict of Interest

Authors declared that, there is no any conflict of interest

References

Alpha, M., Uno, U.E., Isah, K.U. and Ahmadu. (2019). Structural and Electrochemical Properties of AgxSnO1-x/G (0.3≤x≤0.4) Composite Electrode. *European Journal of Scientific Research*. 15, 14, 479-488

Daniel, T.O Uno, E.U., Isah, K.U. and Ahmadu, U. (2020). Tuning of SnS Thin Film Conductivity on Annealing in an Open Air Environment for Transistor Application. *East European Journal of Physics*, (2), 94-103

Deshmukh, G.D., Patil, S.M. and Pawar, P.H. (2015). Optical properties of thin Bi_2Te_3 films synthesized by different techniques. *Journal* of *Chemical*, Biological and *Physical* Sciences, 5, 2769.

Ilican, I., Caglar, Y. and Caglar, M. (2008). Preparation and characterization of ZnO thin films deposited by sol-gel spin coating method. *Journal* of *Optoelectronics* and *Advanced Materials*, 10 (200), 2578.

Jeyaprakash, B.G., Ashok, K.R., Kesavan, K and Amalarani, A. (2010). Synthesis and Some of Structural Characterisation of Nano Particles CdO Thin Film. *American* Journal of *Science*, 6

Kasap, S. and Capper, P. (2017) Handbook of electronic and photonic materials. *Springer, Berlin* 2nd edition

Largeot, J.C., Portet, C., Chmiola, J., Taberna, P.L., Gogotsi, Y. and Simon, P. (2008). Confinement, desolvation and electrosorption effects on the diffusion of ions innanoporous carbon electrode. *Journal of American Chemical Society*. 130, 2730.

Nakazawa, K., Itoh, S., Matsunaga, T., Matsukawa, Y., Satoh, Y. and Abe, H. (2014). Effect of dislocation and grain boundary on deformation mechanism in ultrafine- graine interstitial- free steel. *Material Science and Engineering*. 63, 012125

Martinelli, A., Palenzona, A., Putti, M. and Ferdeghini, C. (2009). Microstructural transition in 1111 Oxy-Pnictides. *J.W.Lynn, Pengcheng Dai Physica*. C469.

Mukherjee, A. and Mitra, P. (2015). Structural and optical characterisation of SnS thin film prepared by SILAR. *Material Science-Poland,* 33, 847. https://doi.org/10.1515/msp-2005-0118

Pandolfo, A.G. and Hollenkamp, A.F. (2006). Carbon properties and their role in supercapacitors. *Journal of Power Sources*.; 11, 157-160.

Rajyalakshmi, T., Pasha, A., Khasim, S., Lakshmi, M. and Imran, M. (2020). Synthesis, characterization and Hall-effect studies of highly conductive polyaniline/graphen nanocomposites. *Applied Sciences* (2020) 2:530. https://doi.org/10.1007/s42452-020-2349-4

Siamak, P.J., Alagarsamy, P., Boon, T.G., Hong, N.L. and Nay, M.H. (2015). Influence of particle size on performance of Nickel nanoparticles-based supercapacitor. *RSC Advances*. 5, 14010- 14019.

Skoog, D.A., West, D.M., Holler, F.J. and Crouch, S.R. (2016). Principles of Instrumental Analysis, Seventh Edition. USA: Cengage Learning.

Uwe, H. and Neil, G. (2011). The Scherrer equation versus the Debye-Scherrer Equation. *Nature Nanotechnology*, 6, 534